RSC Advances

Preferential binding of anticancer drugs to triplex DNA compared to duplex DNA: A Spectroscopic and Calorimetric study

Journal:	*RSC Advances*
Manuscript ID	RA-ART-02-2016-003514.R1
Article Type:	Paper
Date Submitted by the Author:	20-Mar-2016
Complete List of Authors:	Lohani, Neelam; ALL INDIA INSTITUTE OF MEDICAL SCIENCE, BIOCHEMISTRY Rajeswari, Moganty; All India Institute of Medical Sciences, Biochemistry
Subject area & keyword:	Spectroscopy - Analytical < Analytical

RSC Advances

Preferential binding of anticancer drugs to triplex DNA compared to duplex DNA: A Spectroscopic and Calorimetric study

Neelam Lohani[1] and Moganty R. Rajeswari[1*]

Adriamycin and actinomycin are frequently used anti-cancer drugs in the treatment of a variety of human cancers. The resistance and side effects are being the major drawbacks which have been attributed to their non- specific nature of binding to DNA. Therefore, one of the efficient strategies is to target drugs to sequence/and structure specific DNA regions so that higher potency can be achieved. We have chosen a positive regulatory region (-183 to-165 from transcription start site) in hmgb1 gene, as sequence specific target and also made DNA triplex (of the same region) as a structure specific target for anti-cancer drugs and studied the conformational and binding characteristics by using UV-VIS absorption, circular dichroic and fluorescence, Fourier transform infrared spectroscopy and Isothermal titration calorimetry. Binding results showed that in presence of the triplex forming oligonucleotide, DNA triplex formed by the target DNA had higher binding affinity to the drugs as compared to the DNA duplex alone. The results suggest that anti-gene approach of DNA triplex in combination with anti-cancer drug as a preferential option in achieving higher efficacy. Further, the DNA triplex structure-specific target can alleviate the unwanted side effects of anti-cancer drugs.

1.0. Introduction

High mobility group box1 (HMGB1) is a non histone chromosomal protein named for its characteristic rapid mobility in polyacrylamide gel electrophoresis (PAGE). Its role in biology and disease was the central topic of discussion in Merinhoff world congress in New York in October 2013 sponsored by Journal of Internal Medicine (JIM) and recently at 7th International symposium on DAMPS-HMGB1 Meeting in Germany, University Hospital Bonn from 10th Sep to 12th September 2015 .The biological activity of HMGB1 depends on its cellular localization. Under physiological condition it is typically localized in the nucleus and act as a chromosomal architectural protein in transcription regulation, replication, repair, and recombination as well as in chromatin remodelling[1] .During cell activation, injury or death it is released into the extracellular matrix, where it acts as a proinflammatory cytokine mediating a broad range of

inflammatory, immune and chemoattractant function by binding to specific cell-surface receptors[2]. Accumulating evidence suggest that HMGB1 dysfunction is associated with all hallmark of cancer as proposed by Hanahan and Weinberg et al., 2011[3]. Moreover HMGB1 have been found to be a regulator and a prognostic marker of malignant tumourigenesis, proliferation, and metastasis and its overexpression compared to normal cells and cytoplasmic localization is associated with poor clinical pathology in various human cancers including skin cancer, colon cancer, liver cancer, cervical cancer, prostate cancer, colorectal, pancreatic cancer, ovarian cancer, breast cancer etc[4]. In view of the function and regulation of HMGB1 protein in cancer biology described above, designing HMGB1 inhibitors might be a useful therapeutic strategy for the treatment of cancer. Apart from antibody, herbal products and small molecules strategy to target HMGB1 in cancer cell, several antisense and RNA interference (RNAi) have been used in experimental cancer research[5].

1. Department of Biochemistry, All India Institute of Medical Sciences, New Delhi, (INDIA)
* To whom correspondence should be addressed: rajeswari3011@hotmail.com

The alternative approach is interfering with gene replication or transcription using chemotherapeutic drugs that bind DNA and inhibit the polymerase and topoisomerase activity. The major drawback of most of these drugs is that they bind non sequence specifically to DNA and are very toxic to normal healthy cells and cause unwanted side effect and resistance. Therefore, one of the efficient strategies is to target drugs to sequence and structure specific DNA regions so that higher potency can be achieved. The sequence specific recognition of DNA duplex using a third strand synthetic triplex forming oligonucleotide (TFO) has gained enormous attention due to potential application in therapy[6], biotechnology[7] and diagnostic [8]. In the intermolecular triplex system, the third stand or the triplex forming oligonucleotide bind to DNA in the major groove via Hoogsteen base pairing and control the transcription of target gene through blocking the binding of transcription factor or inhibition of RNA polymerase[9]. However, the DNA triplex (Ka~ 10^7) is not as stable as its corresponding duplex (Ka~ 10^8). Consequently, various attempts to enhance the stability of DNA triplex in the past have been explored. Of the compounds tested, the intercalators' coralyne [10] , indoloquinoline drug [11], berberine analog [12], acridines [13] , anthroquinones [14] , Ethidium [15] , naphthoquinolines [16], quinoxaline stabilize the triplex. The addition of multivalent cations to compensate for the charge repulsion between strands [17], synthetic modification of deoxyribose sugars, the nucleobases, or the phosphodiester backbone [18], and covalent attachment of DNA intercalators to the third strand has been found successful [19] [20] in triplex stabilization. So far TFO mediated transcriptional inhibition have been achieved in integrated *hiv-1provirus* [21], *survivin* [22], *tie-1* [23], *bcl-2* [24], *c-met* [25] and more recently in *c-Myc* [26] *androgen receptor gene* [27]. However, the anti-gene strategy via triplex forming oligonucelotide (TFO) in combination with anti-cancer drugs to achieve the transcriptional inhibition of hmgb1 gene has not been attempted yet. Effect of TFO (Triplex forming oligonucleotide) on the regulatory region of hmgb1 gene can assist in understanding the importance of potential anti-gene molecule against malignancies associated with the overexpression of HMGB1. Our previous work has

shown the remarkable ability of adriamycin[28] and actinomycin [29] in increasing the stability of duplex DNA in the promoter region of *hmgb1*. Herein we report our observation regarding the role of two anticancer drug adriamycin (ADM) and actinomycin-D (ACT) as a (25R*R●Y) triplex specific ligand to target gene with high structural and sequence specifically as compared to DNA alone. The triplex targeting site (TTS) in hmgb1 gene was identified by two web based search tool and out of many potential TTS obtained from the software we selected the one from the promoter region between -183 to-165(25mer) from transcription start site (**Figure 1**) and designed triplex forming oligonucleotide (19mer) according to antiparallel Hoogsteen base pair mechanism to form 25R*R●Y triplex. Binding mechanism of adriamycin and actinomycin to nucleic acid is via intercalation and intercalation- cum- minor groove binding respectively. The *in-vitro* binding study between drug and nucleic acid was done using spectroscopic (UV-visible absorption spectroscopy, fluorescence, circular dichroism, and Fourier transform infrared spectroscopy and Isothermal titration calorimetric technique.

2.0. Material and methods

2.1. Materials.

DNA oligonucleotides were purchased from IDT (CA, United States of America). Concentration of the DNA stock solution were determined spectrophotometrically using molar extinction coefficient at 260nm derived from nearest neighbour method. Sample for triplex was prepared in buffer containing 10mM sodium cacodylate, 120mM NaCl and 10mM MgCl$_2$ adjusted to pH 7. HPLC water was used in the preparation of desired aqueous solution. Adriamycin (Sigma) and Actinomycin –D drug (Sigma-Aldrich Corporation, USA) were dissolved in the same buffer as used for DNA samples.

2.2. Design of triple-helical DNA targets in *hmgb1* gene

The structure of *hmgb1* gene and sequence of target sites and TFO are shown in **Figure 1.** Two web-based search tools

were used to find potential triplex targeting sequence or polypurine track in hmgb1 gene in human genome. The sequences were designed using TTS mapping[30] and MD Anderson method (web-based search engine for triplex-forming oligonucleotide target sequences)[31], in an antiparallel base pairing fashion to purine rich DNA promoter region of HMGB1. A total of 23 and 28 potential triplex targeting sites (TTS) were obtained from TTS mapping and MD Anderson method respectively in intron, exon and promoter region of *hmgb1*. Out of all these potential triplex targeting sites we selected the one present in promoter region **(25Y) 5'CCT CTG CCT CTG CCT CTC CCG CCT C3'and (25R) 3'GGA GAC GGA GAC GGA GAG GGC GGA G 5'** fulfilling the following criteria, so that TFO can bind to this target with a very high affinity;(1) The length of TTS to be greater than 15. (2) Guanine percentage in the TTS >50%. (3) The sequence was NCBI Blast for uniqueness.(4) No long tracks of adenine as it will aid in construction of A-DNA.(5)No long stretches of guanine as it hinder the triplex formation. The TFO (19R) **(5'GGA GAG GGA GAG GGG GGA G3** was designed according to antiparallel hoogsteen base pairing to target 25RY duplex. The presence of any type of self-structures (like duplex, triplex or quadruplex etc.) formed if any, by any of the oligonucleotides was checked independently of all three i.e. of 25R, 25Y and TFO by performing slow UV melting experiments. The results reveal the absence of any thermal transition and ruled out the existence of ordered conformations.

2.3. UV-Visible absorption Spectroscopy

All UV absorbance, titration and melting experiment were performed in triplicate using a JASCO-660 UV−VIS spectrophotometer equipped with pelteir with 1 cm path length quartz cells. Triplex DNA absorbance at 260 nm was recorded in the temperature range of 20−90 °C with 1ºC/m. The Tm value was taken as the midpoint of the melting transition as determined by the maximum of the first-derivative plot of the heating curve using Origin 6 software. For the preparation of 25R*R•Y triplex, 25RY DNA duplex was mixed with equal moles of the 19R TFO and heated to

90ºC for 10 min and then allowed to anneal by slow cooling at the rate of 1.0ºC/min. The solution of adriamycin and actinomycin was prepared fresh and their concentration was estimated spectrophotometrically by using molar extinction coefficient at ε_{480} 10,690 and ε_{440} 24800 respectively. All buffer solutions were degassed using a degassing station of TA instrument (Waters). The final pH was adjusted to 7.0.

Data Analysis

 The UV-VIS titration results were expressed in the form of Scatchard plots as r/Cf versus r is the number of drug molecule bound per mole of nucleotide (duplex or triplex) and Cf is the molar concentration of the free drug using the following equation.

$$C_f = C_t \frac{(A/A_o - P)}{1-P} ; \quad C_b = C_t - C_f, \quad P = \frac{A_b}{A_o} \quad .... \text{Equation 1}$$

Where P denotes the ratio of the absorbance of completely bound to the free drug and   A   and A_o are the absorbance of drug in the presence and absence of nucleic acid. Further analysis of the plot was done using Mc-Ghee-Von Hippel equation [32] using Origin 6.0 software (Origin Laboratories, Northampton, MA) that determine the best fit value of Ka (binding constant) and n (number of nucleotide occluded after the binding of a single-drug molecule).

2.4. Circular dichroism spectroscopy

Circular dichroic spectra of DNA triplex in presence and absence of the drugs were recorded in JASCO J-810 (200-700nm) spectropolarimeter equipped with a temperature controller at 25ºC using a 1mm optical length quartz cuvette at various D/N (drug/nucleic acid). Each CD spectrum was collected after averaging over at least 3 accumulations using a scan speed of 100nm min^{-1} and a 1sec response time. All spectra were blank corrected. The CD melting curves of duplex and triplex were determined by following the molar ellipticity at 270nm and 265nm wavelength respectively (the characteristic peak given by B-DNA duplex and triplex DNA).

2.5. Florescence Spectroscopy

Fluorescence data was recorded in Cary Varian spectrofluorometer (Serial no. EL07064176) with an attached temperature controller in a fluorescence free quartz cuvette of 1cm path length using a slit width of 5nm/5nm (exi/emi) and scan speed of 100nm/sec. Aliquots of dissolved oligonucleotides were titrated into a 1cm cuvette with the drug solutions at 25°C. The excitation wavelength of adriamycin and actinomycin is 480nm and 380 nm respectively. The measurements were made over a period of time sufficient to ensure attainment of equilibrium

2.6. Fourier transform infrared (FTIR) spectroscopy

FTIR spectra were recorded on VARIAN-660-IR spectrophotometer equipped with deuterated triglycine sulphate (DTGS) detector and KBr beam splitter. These detectors operate at ambient temperatures and provide adequate sensitivity for most routine applications. An ideal beam-splitter transmits and reflects 50% of the incident radiation. For the mid-IR region the beam splitter is usually made of KBr with a germanium-based coating that makes it semi-reflective. The spectra were recorded using horizontal attenuated total reflection (HATR) crystal which uses a property of total internal reflection resulting in an evanescent wave enables samples to be examined directly in the solid or liquid state without further preparation. All the samples were scanned in the range of 2400-700 cm^{-1} by averaging 256 scans with a resolution of 4cm^{-1}. All the spectra were normalized after baseline correction. Background spectra were collected before each measurement. A spectrum of buffer solution was recorded and subtracted from the spectra of DNA triplex and drug –triplex DNA complexes. A satisfactory water subtraction is achieved when flat baseline around 2200cm^{-1} is produced, where water combination band are present.

2.7. Isothermal titration Calorimetry

All isothermal titration calorimetry experiments were performed using a Nano isothermal titration calorimeter, TA instruments, Waters (USA) at 298K and Nanoanalyze software was used for data analysis. All samples were dissolved in10mM Sodium Cacodylate buffer containing 120mM NaCl and 10mM MgCl$_2$, pH 7.0 at 25°C and degassed prior to titration. The smaller first injection volume (1.0 µL) was omitted before data analysis. Subsequent titration steps involve injections of 50µl degassed drugs/TFO solution injected from a rotating syringe (250 rpm) into the isothermal sample chamber containing the triplex/duplex solution (300µl). Blank titration were conducted by injecting the drugs/TFO into buffer under identical experimental conditions and was subtracted from corresponding heat of the drugs/TFO–triplex/duplex reaction to give the heat of drugs–triplex or TFO-duplex binding. The resulting corrected heat were plotted as a function of the injections and fitted with various model to calculate the thermodynamic parameters including molar binding enthalpy change (ΔH°) and entropy change (ΔS°) together with the number of binding sites (n) and the affinity constant (Ka).The Gibbs free energy change (ΔG°) was calculated according to the relationship.

$\Delta G° = -RT \ln Ka$ (R =1.9872 cal mol^{-1}K^{-1}; T = 298 K)

3. Result and discussion

3.1 Spectroscopic and calorimetric evidences for formation of Triple Helical Structures

The formation of 25R*R●Y DNA triplex containing duplex (25RY) and TFO (19R*) was confirmed from CD, FTIR, ITC & thermal melting studies. All the experiment were done at 150 mM salt concentration containing 120 mM NaCl ,10mM Sodium cacodylate buffer and 10mM MgCl$_2$ at pH 7.0 at 298K.

3.1.1. Stoichiometry of the Complex Forming TFO and Duplex

The stoichiometry of the interacting duplex with the TFO was determined by continuous variation method[33]. **Figure 2** presents the change in UV absorbance at 260nm induced by successive addition of increasing mole fraction of TFO to duplex while keeping the total DNA concentration constant 3µM. A clear inflection point near mole fraction 0.5 characterizes stoichiometry of 25RY and TFO (19R) to be

one-to-one. Therefore, the combination of the 25RY duplex and 19 R results in the formation of a triplex complex

3.1.2. CD Spectroscopy

CD spectroscopy is an important tool to monitor the conformational changes and formation of non-canonical DNA structure. The CD spectra of deoxyribonucleotides depend on the primary sequence because of different conformation properties[34]. The CD spectra of triplex and its corresponding duplex and TFO were recorded at a concentration of 1μM each (**Figure 3**). The intrinsic CD spectra of the duplex is characterized by a positive band at 270 nm and a negative band in the 240 nm ,212nm and 220nm regions which corresponds to the usual B form of DNA duplex[28] .These marker band appear due to helical arrangement of its sugar phosphate backbone and nitrogenous bases. The positive band at 270nm appears due to right handedness of B-DNA helix while the negative band at 240nm is due to stacking interaction between nucleic acid bases[35]. The other negative band at 212nm and 220nm is due to deoxyribose sugar-nitrogenous base interaction and hydrogen bonding interactions respectively. The CD characteristics of the triplex is remarkably different from those of the duplex and the TFO which has two positive bands 260 nm and 208nm, followed by a negative band at 240 nm . The CD spectrum of triplex is produced by the sum of the component Duplex and TFO spectra as reported by Plum et al., 1990[36]. A strong positive band at 265nm and negative band at 240nm for 25R*R●Y triplex was observed on binding of 25RY duplex and 19RTFO.The Complex has additive effect of both 25RY and 19 R .i.e. the band at 212nm in duplex and 208nm in TFO vanish with complexation while of 240nm becomes stronger.

3.1.3. Thermal Denaturation Studies

UV-visible and CD spectroscopic methods were employed to probe the temperature-dependent absorbance/ellipticity changes of 25R*R●Y DNA triple helices. The UV melting studies deduced from the absorbance versus temperature profile demonstrated a characteristic biphasic transitions

(**Supplementary figure ,S.F1a**); the first transition at low Tm value (Tm$_1$= 45±1ºC) represents the melting of the Hoogsteen base paired TFO strand from the Watson-Crick base paired DNA duplex while the second transition at higher Tm value (Tm$_2$= 79±2ºC) represents the dissociation of the DNA duplex to the single strands. The biphasic curve is indicative of the 25R*R●Y triplex formation as Watson–Crick bonding is more stable as compared to the Hoogsteen base pairing found in triplex. The CD melting result were corroborated with UV-VIS melting experiment which shows similar melting temperature with biphasic transition (**S.F 1b**).

3.1.4. Vibrational spectroscopy Analysis

FTIR spectroscopy helps to characterize the nucleic acid structures and conformations in double and triple helices using marker bands. FTIR spectra of free 25RY duplex, 19R TFO and the resulting triplex are shown in **S.F 2** from 1800–700 cm^{-1} spectral region. The spectral region from 1800–1500 cm^{-1} attributes to base pairing and stacking vibration of the nucleic acid[37]. Region from1500–1250 cm^{-1} reflects the vibrational coupling between the base–sugar, glycosidic bond rotation, backbone conformation and sugar pucker. Marker band from 1250–1000 cm^{-1} and 1000– 800 cm^{-1} represent vibrations along the backbone conformation and sugar puckering modes respectively[37].

3.1.4.1. Base Residue Frequency Region

The double-helix spectrum (**S.F. 2**) shows two intense IR bands located at 1689 and 1651 cm^{-1} are classically assigned to the C6=06 of guanine and C2=02 of cytosine stretching vibrations. These two bands are observed to be slightly shifted to higher wavenumbers 1687cm^{-1} and 1655cm^{-1} in IR band of triplex which is evident for the interaction of the TFO with the duplex. The band at 1533 cm^{-1} in TFO is assigned to cytosine residue involving motion of the N3 in cytosine ring atom is very sensitive to Watson crick base pairing. Upon binding of the TFO to the Duplex in the major grove a decrease of the relative intensity of this absorption band is observed. A new band is observed in the IR spectra of triplex

at 1715cm^{-1} is assigned to the unbound C6==06 stretching vibration of the third-strand guanosine residues involved in the dG*dG.dC triplex. The band observed at 1687 cm^{-1} in 25R*R●Y correspond to   purine*purine–pyrimidine triple helix with a mixed A and G sequences in the TFO, characteristic of the reverse Hoogsteen type G*G–C and A*A–T triplets[37]. The band at 1493cm-1 attributes to imidazolic ring vibrations of purine in DNA and depends on the bending of N7C8H[37].Any Interaction on N7 site or change in hydration in the major groove of nucleic acid structures upon triplex formation cause a shift in the position of this band to 1490cm^{-1}.

3.1.4.2. Glycosidic Bond and Sugar conformation frequency Region

Sugar conformations and the base-sugar orientations marker bands in triple helical structures are found between 1250 to 1500 cm^{-1} spectral region[38]. The marker band for *anti* conformation of glycosidic bond vibration is characterized by an absorption band observed around 1377 cm^{-1}, whereas the syn-type conformation is reflected by an absorption band observed around 1355 cm^{-1} [37]. The spectra of the triplex discussed here show a vibration band at 1377cm^{-1} indicating that all the glycosidic linkage of the triplex is in anti conformation. This observation corroborates the molecular modelling calculations to predict the glycosidic bond conformation of C. A. Laughton and S. Neidle that the conformation of glycosidic bond is anti in presence of polar solvent and is syn if the calculation is performed with a dielectric constant mimicking the shielding effects of water[39]. The anti base/sugar position in an antiparellel triplex has also been reported by Radhakrishnan using NMR Spectroscopy [40]. The S type geometry of sugar pucker band in DNA around 1420cm^{-1} band, arising from a coupling between vibrations of the purine imidazole ring and sugar deformations acts as a marker for B-form helices, and can be used in conjunction with the 1373 cm^{-1} band to identify B-form geometry of 25RYdouble helix. The band at 1340cm^{-1} and 1418cm^{-1} in 25R*R●Y is characteristic of adenine and guanosine residue with an S-type (B-family form C2'endo/anti geometry)

geometry of sugar pucker ring which prove the antiparallel triplex to be in B-form helix conformation.

Another region of FTIR spectrum which is sensitive to sugar conformation in triple helices is found between 900 cm^{-1} to 750 cm^{-1} spectral region. The North-type sugar conformation(A family form nucleic acids) present an absorption band around 866 cm^{-1}, whereas the   band for South-type sugar conformation(B family form nucleic acids) is located around 836 cm^{-1}. In a parallel triplex both N type and S type sugar conformation have been known to exist[37]. Whereas in triplexes containing deoxyribose sugars in all three strands in antiparallel orientation only South-type sugars are detected as shown by the absorption band at 836 cm^{-1}.

3.1.4.3. Backbone frequency region

The band at 1000 - 1250 cm^{-1} is assigned to sugar–phosphate vibrations that give rise to marker bands sensitive to nucleic acid backbone conformation (A-, B- or Z-form). The band observed at 1086cm^{-1} and 1220 cm^{-1}, is due to symmetric (C5-O5) and asymmetric phosphate stretching vibration and is the backbone evidence of the B-type helical conformation. The infrared features at 968 and 1052 cm^{-1} emerge due to stretching vibrations of deoxyribose sugar vibrations due to C=C and C=O stretching in the spectrum of triplex DNA. The bands at   894, 780, and 726 cm^{-1} are attributed to deoxyribose ring stretching vibrations which shows minor change in wavelength shift[41].

3.1.5. Thermodynamic Analysis of Triplex Formation

Isothermal titration calorimetry (ITC) was employed to understand the thermodynamics of the complex formed upon binding of TFO (19R*) to TTS (25RY). Isothermal titration calorimetry is an effective tool to enable the direct determination of the molar binding enthalpy change(ΔHº), entropy change (ΔSº) and Gibbs free energy change (ΔGº) together with the number of binding sites (N) and the affinity constant (Ka) and these are not dependent on the spectroscopic changes that occur during the binding event. The representative ITC profiles for the binding of triplex

forming oligonucleotide (TFO) to DNA duplex is presented in **S.F. 3**.The energetic was calculated at 298K. Each of the heat burst spike corresponds to a single injection of 2.5μl containing 100μM TFO into the 5μM DNA solution (300μl) that was corrected by subtracting the corresponding dilution heats derived from a titration of identical amounts of TFO solution into buffer alone. The areas under these heat burst spikes were determined by integration to yield the associated injection heats. The lower panel of the figure represents normalized heat, plotted as a function of the injections. The data points reflects experimental injection heats while the solid lines represent the calculated fits of the data based on independent binding model .The binding data showed a strong exothermic binding event and resulted in change in thermodynamic property (ΔH^o) = -57 ±3 kJ/mol, (ΔS^o) = -40 J/mol k, (ΔG^o)= -10.6 kcal/mol, binding affinity Ka =7.5±3×10^7 and stoichiometry to be 1±0.1. The binding is favoured by both negative enthalpy and entropic changes. High ΔS value for 25R*R●Y triplex formation as compared to duplex (-2218 J/mol k) formation might be partly due to the solvent effect as more water molecule are freed on the formation of 25R*R●Y triplex that involves binding of the 19-merTFO within the major groove of the 25-mer duplex target and should result in a well-defined 1:1 complex in line with the ITC data.

3.2 Complex formation study upon titration of 25R*R●Y triplex with Actinomycin-D and Adriamycin.

3.2.1. Absorption spectral titration results

Figure 4a & b shows the absorption spectral changes of 10μM ADM and ACT in presence of increasing concentration of 25R*R●Y DNA triplex. Adriamycin (ADM) and actinomycin (ACT) have characteristic absorption spectra in the 320–600 nm regions with peak maxima around 480nm and 440 nm, respectively. Upon progressive addition of small aliquots of triplex DNA to the ADM (from N/D ratio 0 to 0.2) and ACT (from N/D ratio 0 to 0.4) drug solution, the absorption maxima exhibit significant (55% in case of ACT

and 64% in case of ADM) hypochromic and (8 to 10nm)bathochromic changes . Such spectral changes have been observed for various drugs involved in intercalation with the nucleic acid [12] and are due to interaction between π electron cloud of aromatic chromophore and base pair of DNA triplex. As can be seen from aromatic ring B and C (**Figure 1**) of adriamycin and the phenoxazine ring system of ACT that can be expected to behave in quite intercalative mode. The effects of the corresponding duplex on the absorption spectra of drugs were grossly similar to that of triplex under identical conditions but the hypochromic changes (25% in case of ACT and 40% in case of ADM) were smaller compared to the triplex(**Table 1**).

Scatchard plot of r/Cf versus r (*inset* **Figure 4**)derived from titration curve was analyzed to determine the binding constant and the number of nucleotide occluded after the binding of a single-ADM /ACT molecule with triplex and their corresponding duplex under identical solution conditions. The binding isotherms for 25R*R●Y triplex and corresponding 25RY duplex (not shown) are nonlinear indicating a non- cooperative binding process. The value of binding constant obtained for triplex- ADM(Ka=1.8 ×10^6 M^{-1}, n=1.7) and triplex-ACT (Ka=5.2 x10^6 M^{-1},n=1.5) interaction was higher than duplex-ADM (Ka=2.0×$10^5 M^{-1}$,n=1.5) [28] and duplex –ACT (Ka=4.2 x10^5,n=2) interaction[29]. This is noteworthy to indicate that ADM and ACT has certain good affinity toward 25R*R●Y DNA triplex compared to its duplex counterpart. The results obtained in this study are comparable to previous data on drug- DNA interaction. The value of binding constant of ADM and ACT for DNA duplex have been shown to be less in other documented reference ; as for ADM to Calf thymus DNA (2.5x10^4/M) [42] , hmga1 promoter(5.4x10^5/M) [32]and in case of ACT to promoter element of c-met (4-5 x 10^5 M^{-1})[43], G-quadruplex ($2 × 10^5 M^{-1}$) [44].

3.2.2. Spectroscopic study using circular dichroism

Conformational changes of the triplex structure in presence of increasing concentration of anticancer drug were investigated

from circular dichroism studies (**Figure 5a, b**). The CD spectrum of triplex is characterized by a positive band at 265nm, a negative band at 240 nm regions (**Figure 3**). In presence of increasing concentration of adriamycin from D/N 0 to 22, a 10nm blue shift at 240nm was observed. In addition, an extrinsic CD band at 210-212 nm and 300nm appeared which shows that bound molecules are in an asymmetric environment. These changes indicate local changes in base-pair geometry and reduction in stacking interaction between the bases of the triple helix upon complex formation. The CD spectra of complexes of actinomycin with triplex DNA (D/N=12) reveal a bathochromic shift of 15nm of the positive CD signal at 265nm, and an isoelliptic point at 275nm was observed along with appearance of B DNA marker peak of 214nm. The perturbation of triplex structures by ACT was indicative of transformation of triplex DNA to duplex DNA. Addition of these drugs to their corresponding duplex brings a very small perturbation in the CD spectrum of the duplex compare to triplex which may be due to the low binding affinity of these drugs to the duplex structure.

3.2.3. Optical thermal melting

Thermal melting experiment is an important tool to examine the effect of small molecules with nucleic acids. The denaturation of the complex, 25R*R●Y triplex-ADM and 25R*R●Y triplex-Act was monitored at 260nm. **Figure 6a and b** illustrates the first derivative from CD melting profile of 25R*R●Y on complexation with ADM and ACT respectively. The thermal melting profiles of triplex showed biphasic transitions, one at a lower temperature corresponds to the dissociation of the TFO to form a duplex and another one at higher temperature is identical to that obtained for the free double stranded form and is associated with duplex melting to single strands. The results shows that the Tm of the first and second melting transition increases with increasing concentration of ADM with $\Delta Tm_1 \sim 9 \pm 2°C$ while for duplex to single stranded the $\Delta Tm_2 \sim 6 \pm 2°C$ at D/N molar ratio 15. The increase in the Tm value is considered as the indicator of stabilizing effect of ADM on triplex by charge neutralization on the phosphate groups through electrostatic screening and

stacking interactions of intercalated ADM molecule. On the other hand the influence of ACT-to-triplex DNA ratios on the triplex melting profiles (D/N=10) showed interesting result with a decrease in Tm value of first transition $\Delta Tm_1 \sim -8 \pm 1°C$ and increase in Tm value of second transition $\Delta Tm_2 \sim 5 \pm 1°C$ which shows that actinomycin can stabilize duplex but not triplex. These results were further confirmed by UV melting experiment and similar results were obtained. Moreover the CD titration results support the destabilizing effect of actinomycin on triplex by conformation change in triplex DNA to duplex DNA.

3.2.4. Fluorescence spectral titration

Changes in fluorescence properties of the drugs were used to monitor the triplex DNA-ligand interactions. Fluorescence titration experiments were performed by adding increasing concentration of 25R*R●Y triplex DNA solution to adriamycin and actinomycin drug solution at various N/D mole ratios. Adriamycin and actinomycin exhibit a strong emission maximum at 590 nm and 480nm when excited at 480nm and 380nm respectively. The fluorescence titration patterns of ADM/ACT-DNA triplex interaction are presented in **Figure7**. Binding to 25R*R●Y DNA triplex and duplex resulted in progressive changes in the intrinsic fluorescence intensity of the drugs, eventually leading to saturation. A significant degree of fluorescence quenching (95%) of ADM at D/N=0.32 was observed with no change in wavelength shift in the maximum emission wavelength. The large fluorescence change strongly suggest an intercalative binding process of ADM with the antiparallel triplex where the drug is efficiently screened from the aqueous solvent in the triple helices. In contrast, at N/D=0.65 actinomycin experience a considerably stronger enhancement of fluorescent intensity upon binding to triplex possibly resulting from sequestration of drug in the region of low polarity such as in minor grooves which are protected from polar aqueous environment. The non polar complex increase the strength of ACT –DNA hydrogen bond compared to DNA water hydrogen bond, thereby providing an additional enthalpy driving force for the binding event. Therefore, the fluorescence data obtained

under these conditions likely reflect intercalation of ADM and intercalation-cum- groove binding mechanism of ACT-D in between base triads of the triplex.

3.2.5. Infrared spectra analysis of triplex-drug complex

FTIR Spectral feature associated with binding of triplex DNA with ADM and ACT are shown in **Figure 8 and 9**. FTIR spectral region from 1800cm^{-1} – 700 cm^{-1} attributes to four major nitrogenous bases, phosphate groups and sugar bands in the spectrum of free triplex.

3.2.5.1. Nitrogen base analysis

The change in intensity and shift in spectral feature of B-form of triplex were examined at different Drug/Nucleotide (D/N) molar ratio. The band at 1688cm^{-1} correspond to purine*purine–pyrimidine triple helix with a mixed adenine and guanine containing TFO. The peak at 1490cm^{-1} and 1295cm^{-1} position is due to in plane stretching vibration of cytosine. The band at 1561cm^{-1} is assigned to ring vibrations of guanine, and has been used to follow the changes in environment of guanine-rich regions in a particular nucleic acid structure[37]. Infrared band observed in the spectrum of free triplex show changes in position of these bands upon binding to ADM/ACT (**Figure 8a &9a**). The triplex band observed at 1688 cm^{-1} shows a shift toward higher frequency at 1697cm^{-1} in case of ADM and up to 1690cm^{-1} in case of ACT. These spectral changes attributes to direct interaction of ADM and ACT to G-G and A-A hoogsteen base paired 25R*R●Y DNA triplex. The band at 1561cm^{-1} shows a decrease in intensity at D/N mole ratio 10 which suggest all the guanine bases in 25R*R●Y DNA triplex are bound by ADM and ACT.

The cytosine band of triplex at 1490cm^{-1} and 1295cm^{-1} show minor shift in frequency upon complexation with ACT& ADM. Moderate shift in guanine and cytosine band are assigned to marker band for intercalation between the base pair. Similarly thymine (T) C2=O2 bonds stretching vibration around 1690cm^{-1} and 1661cm^{-1} is a specific marker for minor

groove binding interaction which was observed on complexation of ACT with triplex at D/N=10. The shift in peak positions is also accompanied by the change in intensity in all 25R*R●Y triplex drug complex. The positive feature observed in the 25R*R●Y –ADM difference spectra [(25R*R●Y solution + ADM solution) – 25R*R●Y solution] at 1720 cm^{-1} and 1490cm^{-1} are due to increase intensity of guanine and cytosine base vibration(**Figure 8b**). Beside these remarkable positive bands, negative band at 1652cm^{-1} was also observed due to decrease in intensity of thymine vibration. These band shift and intensity variation can be attributed to the direct interaction of ADM with heterocyclic bases of 25R*R●Y. On the other hand, the difference spectra of 25R*R●Y -ACT complexes [(25R*R●Y solution + ACT solution)– 25R*R●Y solution] at D/N=10(**Figure 9b**) exhibited infrared hyperchromism of the stretching vibration of guanine band at 1569 cm^{-1} and cytosine band at 1485cm^{-1} along with A-DNA marked band at 1700cm^{-1}. Additional marked infrared hypochromism was observed for stretching vibration of (C2=02) thymine band at 1640cm^{-1}. Besides this, adenine residues underwent no intensity change, at 1605 cm^{-1} .These spectral results suggest the direct interaction of actinomycin with mixed guanine and adenine residues in TFO and cytosine and thymine residues in DNA duplex. Thus these finding demonstrate the binding of actinomycin to be via minor- groove-cum intercalation and adriamycin through only intercalation between base pairs of DNA.

3.2.5.2. Glycosidic Bond and Sugar conformation frequency Region

The peaks at position 1250 to 1500 cm^{-1} are assigned to sugar conformations and the base-sugar orientations. The anti conformation of 25R*R●Y triplex glycosidic bond marker band at 1377cm^{-1} shift to 1379cm^{-1} after binding to ADM and to 1373cm^{-1} after binding to ACT. The difference spectra reveal a positive intensity band at 1382cm^{-1}(ADM) and 1381cm^{-1}(ACT) indicating drug-25R*R●Y complexation. The band at 1418cm^{-1} attributes to S-type (C2'endo/anti geometry) geometry of sugar pucker ring show a slight deviation in the ADM/ACT complex with 25R*R●Y triplex.

In both the cases the band at 1418cm^{-1} shifts to1413cm^{-1} (ADM) and 1417cm^{-1}(ACT). IR band at 836 cm^{-1} (south-type sugar conformation) and 894cm^{-1} (assigned to sugar phosphate stretch) show minor shift of 1-2cm^{-1} upon complexation with adriamycin and actinomycin at D/N ratio 10 along with increase in intensity (positive band at 833-834cm^{-1} and 894-896cm^{-1}) which indicate local perturbation in triplex DNA conformation.

3.2.5.3. Backbone frequency region

In the spectrum of free triplex DNA, infrared bands at 1086cm^{-1} and 1220 cm^{-1} are due to symmetric (C5-O5) and asymmetric phosphate stretching vibration respectively. Minor shift in Infrared band attributed to phosphate symmetric (C5-O5) was observed at 1086cm^{-1} while the band assigned to asymmetric phosphate stretching vibration at 1220cm^{-1} show a downward shift to 1217cm^{-1}and 1218cm^{-1} for ACT and ADM respectively. Additionally positive feature of band at 1218 – 1215cm^{-1} and 1085 cm^{-1} are observed in the difference spectrum of 25R*R●Y triplex ADM and ACT which indicates increase in intensity of phosphate symmetric and asymmetric stretching vibrations. Deoxyribose sugar vibrations in 25R*R●Y triplex due to C=C and C=O emerge at 968 and 1052 cm^{-1}. After addition of adriamycin to the triplex both sugar band shift to 966cm^{-1} and 1055cm^{-1} and show a positive intensity band at 965cm^{-1} and 1059cm^{-1} in the difference spectra. Similarly effect of actinomycin complexation leads to change in band position toward 969cm^{-1} and 1056cm^{-1} along with positive feature at 971cm^{-1} and slight negative feature at 1055cm^{-1} in the difference spectra. Furthermore, other bands at 1019, 894, 780, and 726 cm^{-1} attributed to deoxyribose ring stretching vibrations show minor shift when ADM and ACT interaction with triplex takes place. Spectral feature observed for sugar conformation , phosphate stretching vibration and sugar phosphate backbone suggest minor external binding of adriamycin and actinomycin with sugar –phosphate backbone of 25R*R●Y.

3.2.6. Evaluation of binding sites and thermodynamic Parameters.

All thermodynamic parameters obtained from Isothermal titration calorimetry (ITC) on triplex-drug interaction study are given in **Table 2**. ITC Nano Analyse software provides six built-in curve fitting models each having a unique set of fitting parameters : Independent binding, multiple binding sites, cooperative binding, competitive replacement model, blank (linear) and dimer dissociation. We perform and checked for the best fitting iterations for our data. The best fitting model for the interaction of 25RY/25R*R●Y to adriamycin was multiple binding site model and to actinomycin was independent binding model. Compared to independent binding fit where there is only one association constant of a 1:1 interaction ,the multiple binding site model of a macromolecule with n multiple ligand binding sites can be described by two different association constants. The larger association constant describes the overall behaviour of the n sites, whereas the association constant with lower value takes into account how binding occurs at each site [45]. Thermodynamic parameters of the adriamycin (600μM) binding to triplex DNA differ noticeably from actinomycin (450μM) (**Figure 10**). Based on multiple binding site model, the ITC data of adriamycin-triplex complexation yielded two set of the equilibrium binding constant Ka_1 ($8.5 \pm 3 \times 10^8$ /M) and Ka_2 ($7.2 \pm 5 \times 10^7$ /M) , the binding stoichiometry n_1 (8.0 ± 1) and n_2 (4.9 ± 2),the molar binding enthalpy $\Delta H_1°$ (-159.5 ± 30 kJ/mol) & $\Delta H_2°$(-5 ± 29 kJ/mol), the molar entropy $\Delta S1°$ (-365 J/mol k) & $\Delta S2°$ (131 J/mol k) and $\Delta G1°$ (-12.1 kcal/mol) and $\Delta G2°$ (-10.6 kcal/mol).With their hundred times marked preference for triplex over duplex structures, the adriamycin bind to duplex with Ka_1($1.3 \pm 1 \times 10^5$ /M) and Ka_2 ($5.2 \pm 1.4 \times 10^5$ /M) , the binding stoichiometry n_1 (10 ± 2) and n_2 (7 ± 2),the molar binding enthalpy $\Delta H_1°$ (-172.5 ± 40 kJ/mol) & $\Delta H_2°$ (-137 ± 36 kJ/mol)), the molar entropy $\Delta S1°$ (-480 J/mol k) & $\Delta S2°$ (-350J/mol k) and $\Delta G1°$ (-6.9 kcal/mol) and $\Delta G2°$ (-7.7 kcal/mol). So the overall behaviour of ADM binding to duplex/ triplex was enthalpy driven resulting in positive peaks in the upper plot. The binding has occur by enthalpy entropy compensation that is a characteristic feature of intercalating drug[46]. In case of

ARTICLE

actinomycin interaction with triplex (**Figure 10b**) the ITC data yielded (ΔH^o) =10.5±2 kJ/mol, (ΔS^o) =147 J/mol k, (ΔG^o) = - 7.3 kcal/mol, binding affinity Ka =6.9±0.7X10^5 and stoichiometry to be 5±0.5. On the other hand binding affinity and thermodynamics parameter of actinomycin and duplex complexation gave an association constant Ka= 6±3 x10^4 , a (ΔH^o) = 17.3±2.3kJ/mol, (ΔS^o) = 149.6 J/mol k, (ΔG^o)= - 5.13 kcal/mol and stoichiometry 4± 1. Binding of duplex/triplex to actinomycin was entropic driven with endothermic binding event which have often been associated with variety of DNA groove binders. The extracted negative ΔG° for all experimental values at 298K is a good measure of spontaneity and exclusive ligand binding effects in the duplex/ triplex.

Conclusion

Present study is focused on the binding of two anticancer drugs actinomycin and adriamycin with DNA Duplex and compared with those of their cognitive DNA triplex structures formed by oligonucleotides (TFO). The biophysical characterization by spectroscopic and calorimetric aspects confirmed the binding mode of ADM to be intercalation driven by large and favourable enthalpy and that of ACT to be intercalation-cum-minor groove binding which is entropically driven with a marked preference for triplex over duplex structure in both the cases. However, additional structural information will be needed to know the exact mechanism of action to complement the gene expression perspectives. This study may be useful for the design and developments of TFO- ADM/ACT based therapeutic agents with higher efficacy and stimulate the search for other oligonucleotide sequence and drugs with similar property for gene targeted therapy.

Acknowledgement

References

1. Giavara, S.; Kosmidou, E.; Hande, M. P.; Bianchi, M. E.; Morgan, A.; d'Adda di Fagagna, F.; Jackson, S. P., Yeast Nhp6A/B and mammalian Hmgb1 facilitate the maintenance of genome stability. *Current biology : CB* **2005,** *15* (1), 68-72.
2. Lohani, N.; Rajeswari, M. R., Dichotomous life of DNA Binding High Mobility Group box1 Protein in human health and disease. *Current protein & peptide science* **2016**.
3. Hanahan, D.; Weinberg, R. A., Hallmarks of cancer: the next generation. *Cell* **2011,** *144* (5), 646-74.
4. Kang, R.; Zhang, Q.; Zeh, H. J., 3rd; Lotze, M. T.; Tang, D., HMGB1 in cancer: good, bad, or both? *Clinical cancer research : an official journal of the American Association for Cancer Research* **2013,** *19* (15), 4046-57.
5. Musumeci, D.; Roviello, G. N.; Montesarchio, D., An overview on HMGB1 inhibitors as potential therapeutic agents in HMGB1-related pathologies. *Pharmacology & therapeutics* **2014,** *141* (3), 347-57.
6. Rajeswari, M. R., DNA triplex structures in neurodegenerative disorder, Friedreich's ataxia. *Journal of biosciences* **2012,** *37* (3), 519-32.
7. Simon, P.; Cannata, F.; Concordet, J. P.; Giovannangeli, C., Targeting DNA with triplex-forming oligonucleotides to modify gene sequence. *Biochimie* **2008,** *90* (8), 1109-16.
8. (a) Jain, A.; Wang, G.; Vasquez, K. M., DNA triple helices: biological consequences and therapeutic potential. *Biochimie* **2008,** *90* (8), 1117-30; (b) Schleifman, E. B.; Chin, J. Y.; Glazer, P. M., Triplex-mediated gene modification. *Methods Mol Biol* **2008,** *435*, 175-90.
9. Helene, C.; Thuong, N. T.; Harel-Bellan, A., Control of gene expression by triple helix-forming oligonucleotides. The antigene strategy. *Annals of the New York Academy of Sciences* **1992,** *660*, 27-36.
10. Moraru-Allen, A. A.; Cassidy, S.; Asensio Alvarez, J. L.; Fox, K. R.; Brown, T.; Lane, A. N., Coralyne has a preference for intercalation between TA.T triples in intramolecular DNA triple helices. *Nucleic acids research* **1997,** *25* (10), 1890-6.
11. Riechert-Krause, F.; Autenrieth, K.; Eick, A.; Weisz, K., Spectroscopic and calorimetric studies on the binding of an indoloquinoline drug to parallel and antiparallel DNA triplexes. *Biochemistry* **2013,** *52* (1), 41-52.
12. Bhowmik, D.; Kumar, G. S., Interaction of 9-O-(omega-amino) alkyl ether berberine analogs with poly(dT).poly(dA)*poly(dT) triplex and poly(dA).poly(dT) duplex: a comparative study. *Molecular biology reports* **2013,** *40* (9), 5439-50.
13. Kim, H. K.; Kim, J. M.; Kim, S. K.; Rodger, A.; Norden, B., Interactions of intercalative and minor groove binding ligands with triplex poly(dA).[poly(dT)]2 and with duplex poly(dA).poly(dT) and poly[d(A-T)]2 studied by CD, LD, and normal absorption. *Biochemistry* **1996,** *35* (4), 1187-94.
14. Fox, K. R.; Polucci, P.; Jenkins, T. C.; Neidle, S., A molecular anchor for stabilizing triple-helical DNA. *Proceedings of the National Academy of Sciences of the United States of America* **1995,** *92* (17), 7887-91.
15. Strekowski, L.; Hojjat, M.; Wolinska, E.; Parker, A. N.; Paliakov, E.; Gorecki, T.; Tanious, F. A.; Wilson, W. D., New triple-helix DNA stabilizing agents. *Bioorganic & medicinal chemistry letters* **2005,** *15* (4), 1097-100.

16. Keppler, M.; Zegrocka, O.; Strekowski, L.; Fox, K. R., DNA triple helix stabilisation by a naphthylquinoline dimer. *FEBS letters* **1999,** *447* (2-3), 223-6.

17. Fox, K. R., Targeting DNA with triplexes. *Current medicinal chemistry* **2000,** *7* (1), 17-37.

18. Duca, M.; Vekhoff, P.; Oussedik, K.; Halby, L.; Arimondo, P. B., The triple helix: 50 years later, the outcome. *Nucleic acids research* **2008,** *36* (16), 5123-38.

19. Eick, A.; Riechert-Krause, F.; Weisz, K., Spectroscopic and calorimetric studies on the triplex formation with oligonucleotide-ligand conjugates. *Bioconjugate chemistry* **2010,** *21* (6), 1105-14.

20. Gianolio, D. A.; Segismundo, J. M.; McLaughlin, L. W., Tethered naphthalene diimide-based intercalators for DNA triplex stabilization. *Nucleic acids research* **2000,** *28* (10), 2128-34.

21. Giovannangeli, C.; Diviacco, S.; Labrousse, V.; Gryaznov, S.; Charneau, P.; Helene, C., Accessibility of nuclear DNA to triplex-forming oligonucleotides: the integrated HIV-1 provirus as a target. *Proceedings of the National Academy of Sciences of the United States of America* **1997,** *94* (1), 79-84.

22. Shen, C.; Buck, A.; Polat, B.; Schmid-Kotsas, A.; Matuschek, C.; Gross, H. J.; Bachem, M.; Reske, S. N., Triplex-forming oligodeoxynucleotides targeting survivin inhibit proliferation and induce apoptosis of human lung carcinoma cells. *Cancer gene therapy* **2003,** *10* (5), 403-10.

23. Hewett, P. W.; Daft, E. L.; Laughton, C. A.; Ahmad, S.; Ahmed, A.; Murray, J. C., Selective inhibition of the human tie-1 promoter with triplex-forming oligonucleotides targeted to Ets binding sites. *Mol Med* **2006,** *12* (1-3), 8-16.

24. Shen, C.; Buck, A.; Mehrke, G.; Polat, B.; Gross, H.; Bachem, M.; Reske, S., Triplex forming oligonucleotide targeted to 3'UTR downregulates the expression of the bcl-2 proto-oncogene in HeLa cells. *Nucleic acids research* **2001,** *29* (3), 622-8.

25. Singhal, G.; Akhter, M. Z.; Stern, D. F.; Gupta, S. D.; Ahuja, A.; Sharma, U.; Jagannathan, N. R.; Rajeswari, M. R., DNA triplex-mediated inhibition of MET leads to cell death and tumor regression in hepatoma. *Cancer gene therapy* **2011,** *18* (7), 520-30.

26. Boulware, S. B.; Christensen, L. A.; Thames, H.; Coghlan, L.; Vasquez, K. M.; Finch, R. A., Triplex-forming oligonucleotides targeting c-MYC potentiate the anti-tumor activity of gemcitabine in a mouse model of human cancer. *Molecular carcinogenesis* **2014,** *53* (9), 744-52.

27. Graham, M. K.; Brown, T. R.; Miller, P. S., Targeting the human androgen receptor gene with platinated triplex-forming oligonucleotides. *Biochemistry* **2015,** *54* (13), 2270-82.

28. Lohani, N.; Narayan Singh, H.; Agarwal, S.; Mehrotra, R.; Rajeswari, M. R., Interaction of adriamycin with a regulatory element of hmgb1: spectroscopic and calorimetric approach. *Journal of biomolecular structure & dynamics* **2014,** 1-12.

29. Lohani, N.; Singh, H. N.; Rajeswari, M. R., Structural aspects of the interaction of anticancer drug Actinomycin-D to the GC rich region of hmgb1 gene. *International journal of biological macromolecules* **2016**.

30. Jenjaroenpun, P.; Kuznetsov, V. A., TTS mapping: integrative WEB tool for analysis of triplex formation target DNA sequences, G-quadruplets and non-protein coding regulatory DNA elements in the human genome. *BMC genomics* **2009,** *10 Suppl 3*, S9.

31. Gaddis, S. S.; Wu, Q.; Thames, H. D.; DiGiovanni, J.; Walborg, E. F.; MacLeod, M. C.; Vasquez, K. M., A web-based search engine for triplex-forming oligonucleotide target sequences. *Oligonucleotides* **2006,** *16* (2), 196-201.

32. Akhter, M. Z.; Sharma, A.; Rajeswari, M. R., Interaction of adriamycin with a promoter region of hmga1 and its inhibitory effect on HMGA1 expression in A431 human squamous carcinoma cell line. *Molecular bioSystems* **2011,** *7* (4), 1336-46.

33. Das, A.; Saha, T.; Ahmad, F.; Roy, K. B.; Rishi, V., Dodecamer d-AGATCTAGATCT and a homologous hairpin form triplex in the presence of peptide REWER. *PloS one* **2013,** *8* (5), e65010.

34. Kypr, J.; Kejnovska, I.; Renciuk, D.; Vorlickova, M., Circular dichroism and conformational polymorphism of DNA. *Nucleic acids research* **2009,** *37* (6), 1713-25.

35. Agarwal, S.; Jangir, D. K.; Mehrotra, R.; Lohani, N.; Rajeswari, M. R., A structural insight into major groove directed binding of nitrosourea derivative nimustine with DNA: a spectroscopic study. *PloS one* **2014,** *9* (8), e104115.

36. Plum, G. E.; Park, Y. W.; Singleton, S. F.; Dervan, P. B.; Breslauer, K. J., Thermodynamic characterization of the stability and the melting behavior of a DNA triplex: a spectroscopic and calorimetric study. *Proceedings of the National Academy of Sciences of the United States of America* **1990,** *87* (23), 9436-40.

37. Banyay, M.; Sarkar, M.; Graslund, A., A library of IR bands of nucleic acids in solution. *Biophysical chemistry* **2003,** *104* (2), 477-88.

38. Akhebat, A.; Dagneaux, C.; Liquier, J.; Taillandier, E., Triple helical polynucleotidic structures: an FTIR study of the C+ .G. Ctriplet. *Journal of biomolecular structure & dynamics* **1992,** *10* (3), 577-88.

39. Laughton, C. A.; Neidle, S., Prediction of the structure of the Y+.R-.R(+)-type DNA triple helix by molecular modelling. *Nucleic acids research* **1992,** *20* (24), 6535-41.

40. Radhakrishnan, I.; de los Santos, C.; Patel, D. J., Nuclear magnetic resonance structural studies of A.AT base triple alignments in intramolecular purine.purine.pyrimidine DNA triplexes in solution. *Journal of molecular biology* **1993,** *234* (1), 188-97.

41. Agarwal, S.; Jangir, D. K.; Mehrotra, R., Spectroscopic studies of the effects of anticancer drug mitoxantrone interaction with calf-thymus DNA. *Journal of photochemistry and photobiology. B, Biology* **2013,** *120*, 177-82.

42. Agudelo, D.; Bourassa, P.; Berube, G.; Tajmir-Riahi, H. A., Intercalation of antitumor drug doxorubicin and its analogue by DNA duplex: structural features and biological implications. *International journal of biological macromolecules* **2014,** *66*, 144-50.

43. Singhal, G.; Rajeswari, M. R., Interaction of actinomycin D with promoter element of c-met and its inhibitory effect on the expression of c-Met. *Journal of biomolecular structure & dynamics* **2009,** *26* (5), 625-36.

RSC Advances

ARTICLE

44. Hudson, J. S.; Brooks, S. C.; Graves, D. E., Interactions of actinomycin D with human telomeric G-quadruplex DNA. *Biochemistry* **2009,** *48* (21), 4440-7.

45. Di Cera, E., Thermodynamic basis of site-specific cooperativity. *Biopolymers* **1994,** *34* (8), 1001-5.

46. Chaires, J. B., A thermodynamic signature for drug-DNA binding mode. *Archives of biochemistry and biophysics* **2006,** *453* (1), 26-31.
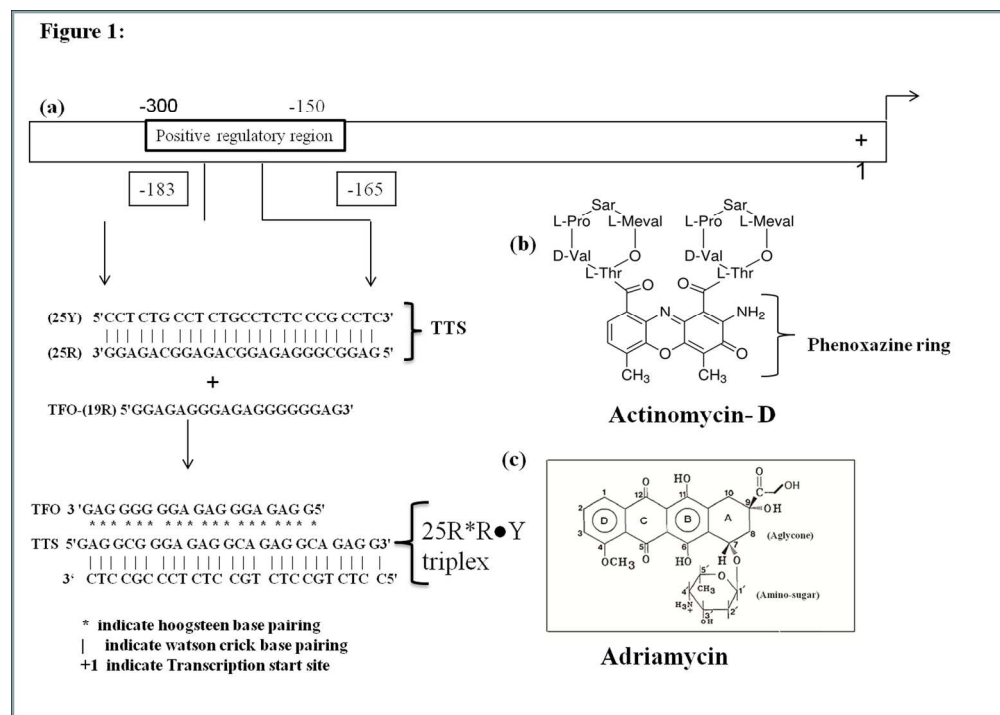
Figure 1: Schematic representation of the structural organization of transcription regulatory region of hmgb1 gene -165 to -183 from transcription start site. The triplex targeting sites and its corresponding triplex forming oligonucleotide (TFO) are also shown.(b) Chemical structure of Actinomycin containing two cyclic pentapeptide lactones and a planar 2-aminophenoxazin-3-one chromophore (B and Q denote the benzenoid and quinoid portions of the phenoxazone ring).(c) Chemical structure of adriamycin containing a planar aglycone chromophore comprising of four fused rings(A, B, C, D) and the amino-sugar ring which is attached to the glycosidic linkage.
181x128mm (300 x 300 DPI)
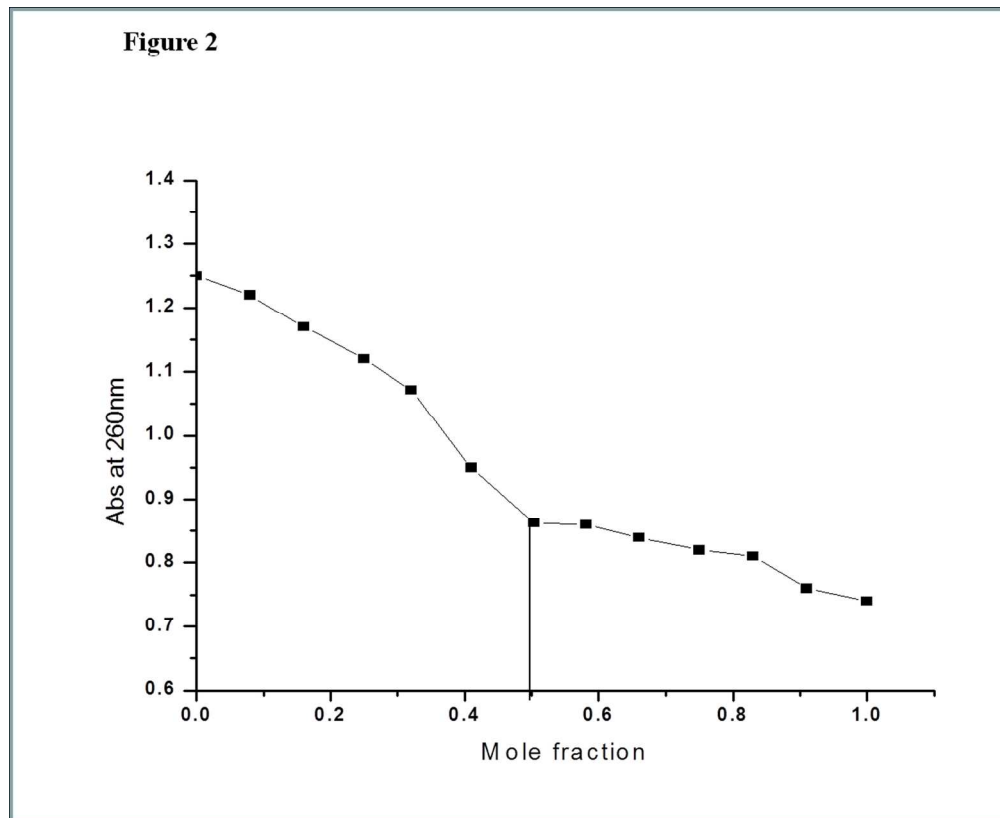
Figure 2: Stoichiometry determination using Job's continuous variations plot for the 19RTFO–25RY DNA
duplex complex at 260nm at various mole fraction of TFO from 0 to 1 keeping the total concentration
of 25RY and 19 R constant at 3.0 µM.
170x139mm (300 x 300 DPI)
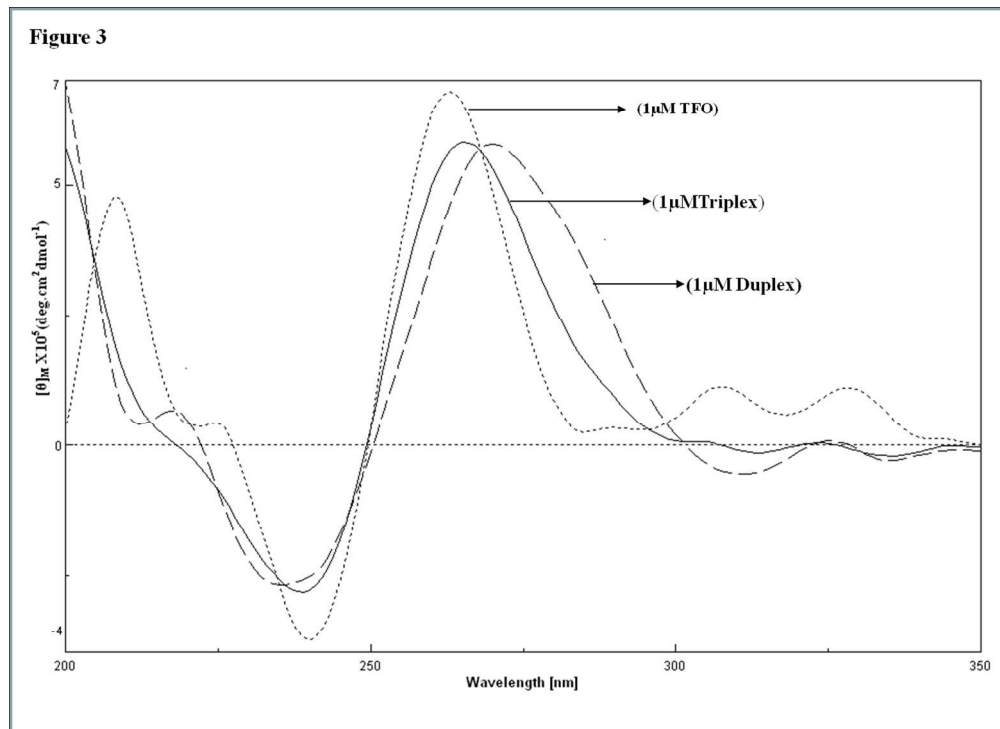
Figure 3: Circular dichroic spectra of 25 RY duplex(Bold dashed line), TFO (19R) (Thin dashed line) and 25R*R•Y triplex(bold line) from 200 -350nm in 10mM Na-cacodylate buffer containing 120mM NaCl and 10mM MgCl$_2$ pH 7.0 at 25°C.
185x134mm (300 x 300 DPI)
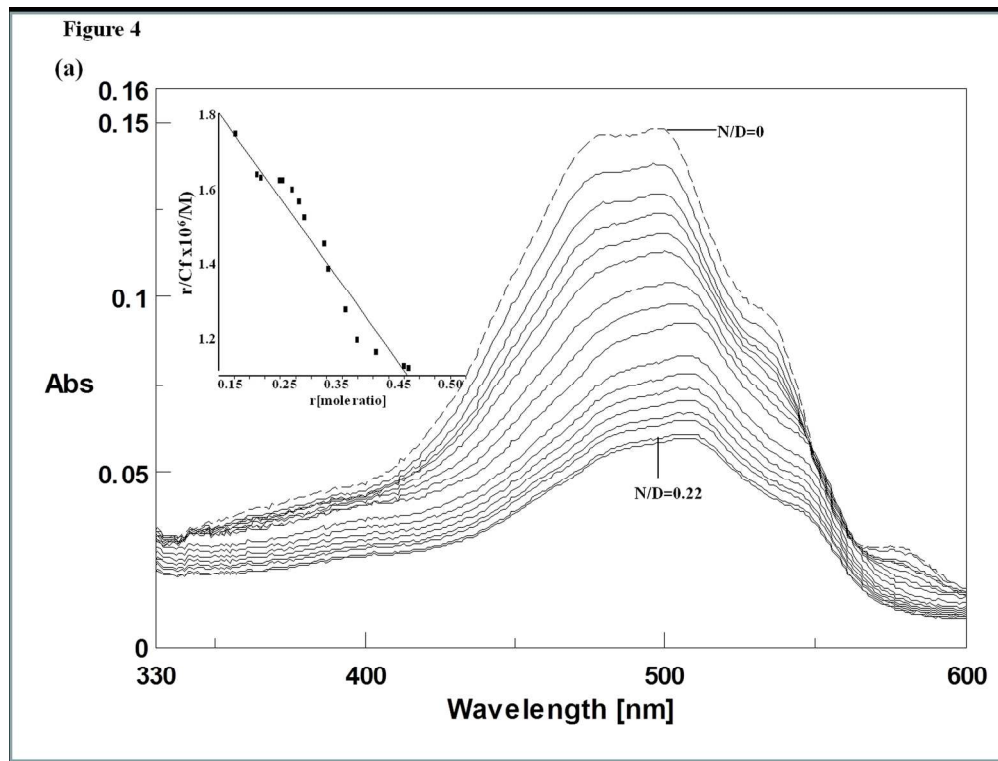
Figure 4: UV-VIS absorption changes of (a)10μM ADM and (b) ACT in presence of increasing concentration of 25R*R•Y DNA triplex at N/D molar ratio from 0.0 to 0.22 and 0.5 respectively where N and D are molar concentration of nucleotide and drug.(Inset Scatchard plot derived from the data of UV-absorption spectroscopy, where 'r' represents the mole ratio of the bound fraction of drug to triplex and Cf is the concentration of the free drug).
192x145mm (300 x 300 DPI)
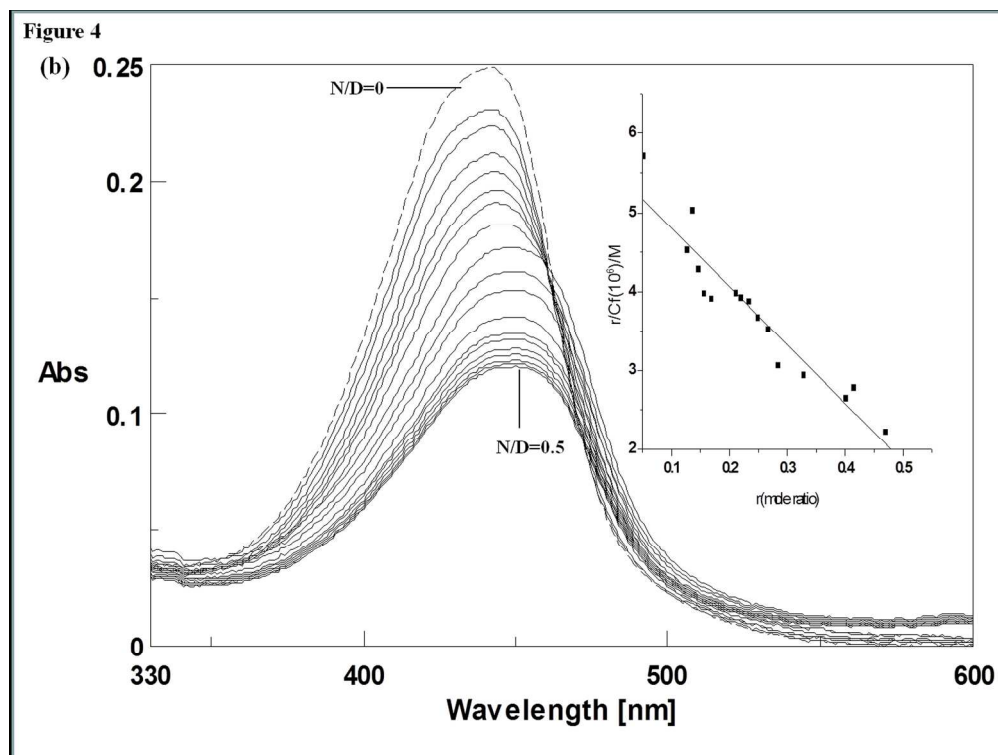
Figure 4: UV-VIS absorption changes of (a)10μM ADM and (b) ACT in presence of increasing concentration of 25R*R●Y DNA triplex at N/D molar ratio from 0.0 to 0.22 and 0.5 respectively where N and D are molar concentration of nucleotide and drug.(Inset Scatchard plot derived from the data of UV-absorption spectroscopy, where 'r' represents the mole ratio of the bound fraction of drug to triplex and Cf is the concentration of the free drug).
191x143mm (300 x 300 DPI)
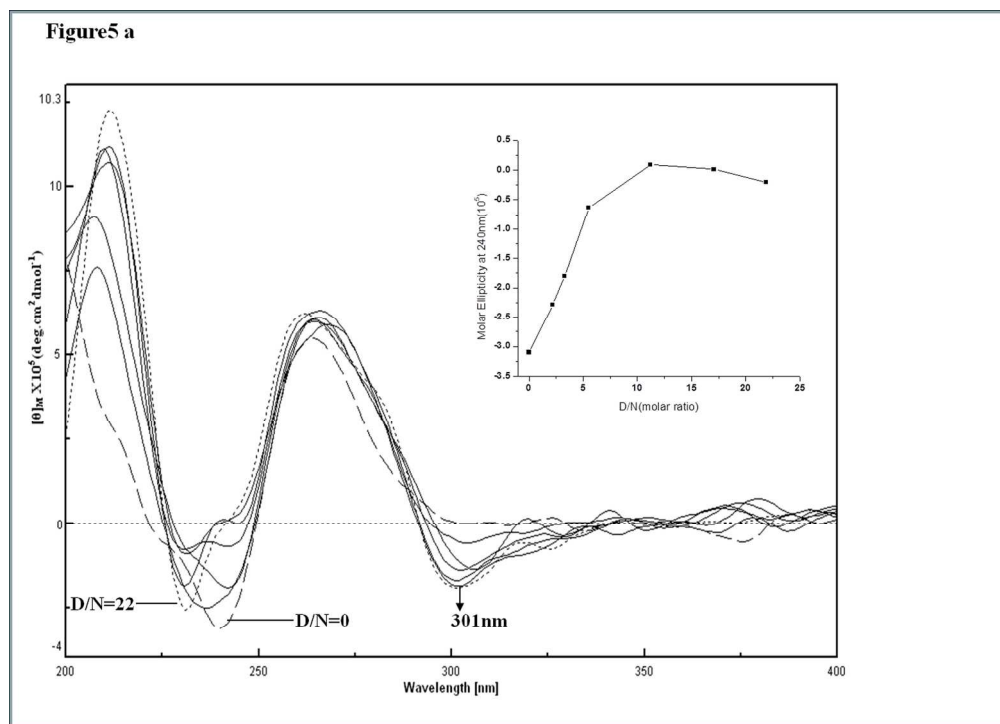
Figure 5: Circular dichroic spectral changes in Triplex (5µM) alone (D/N=0) and in presence of increasing concentration of adriamycin and actinomycin at different D/N mole ratios ranging from(a) 0.0 to22 and (b) 0.0 to 12 respectively. (Inset) Plot of change in molar ellipticity at 240nm as a function of D/N mole ratios. 183x131mm (300 x 300 DPI)
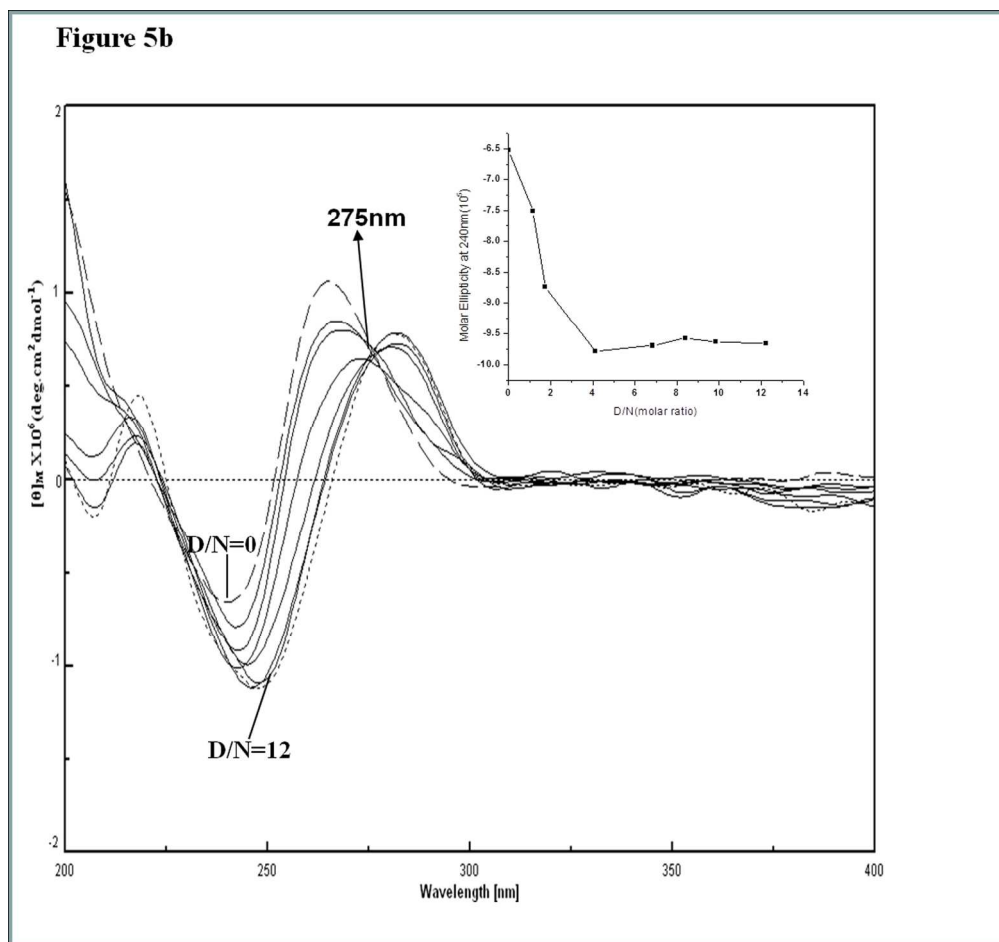
Figure 5: Circular dichroic spectral changes in Triplex (5μM) alone (D/N=0) and in presence of increasing concentration of adriamycin and actinomycin at different D/N mole ratios ranging from(a) 0.0 to22 and (b) 0.0 to 12 respectively. (Inset) Plot of change in molar ellipticity at 240nm as a function of D/N mole ratios. 183x171mm (300 x 300 DPI)
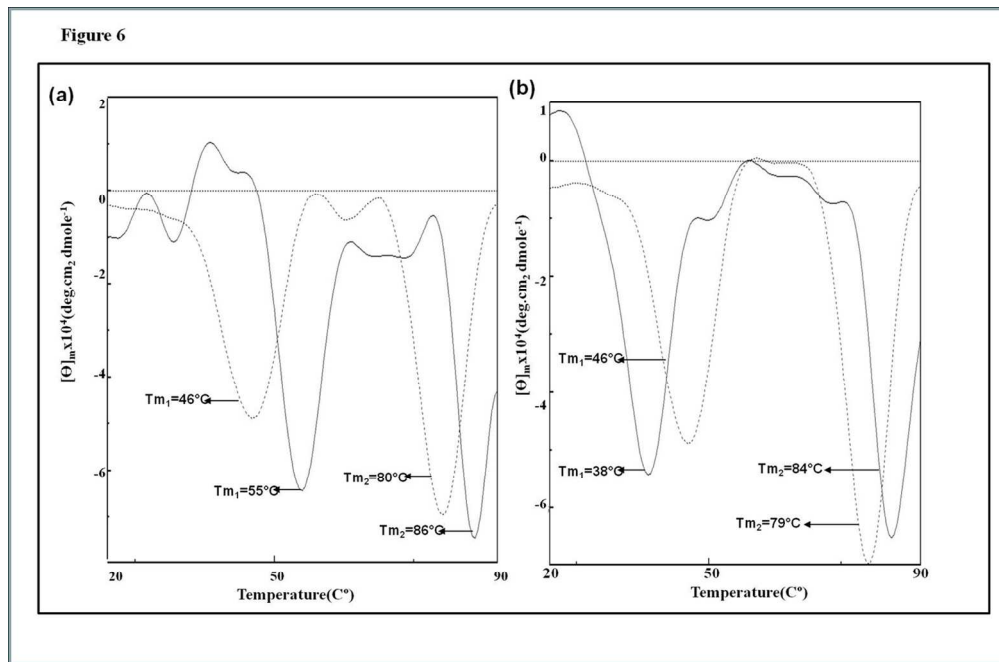
Figure 6: CD melting profile of 1.0μM 25R*R●Y alone (thin dashed line) and complexed with(a) ADM (bold line) and (b) ACT (bold line) from 20 to 90ºC at 260nm. Tm_1 represent melting of the 19R TFO from 25RY duplex while the second transition at higher Tm_2 value represents the dissociation of the duplex to the single strands.
168x110mm (300 x 300 DPI)
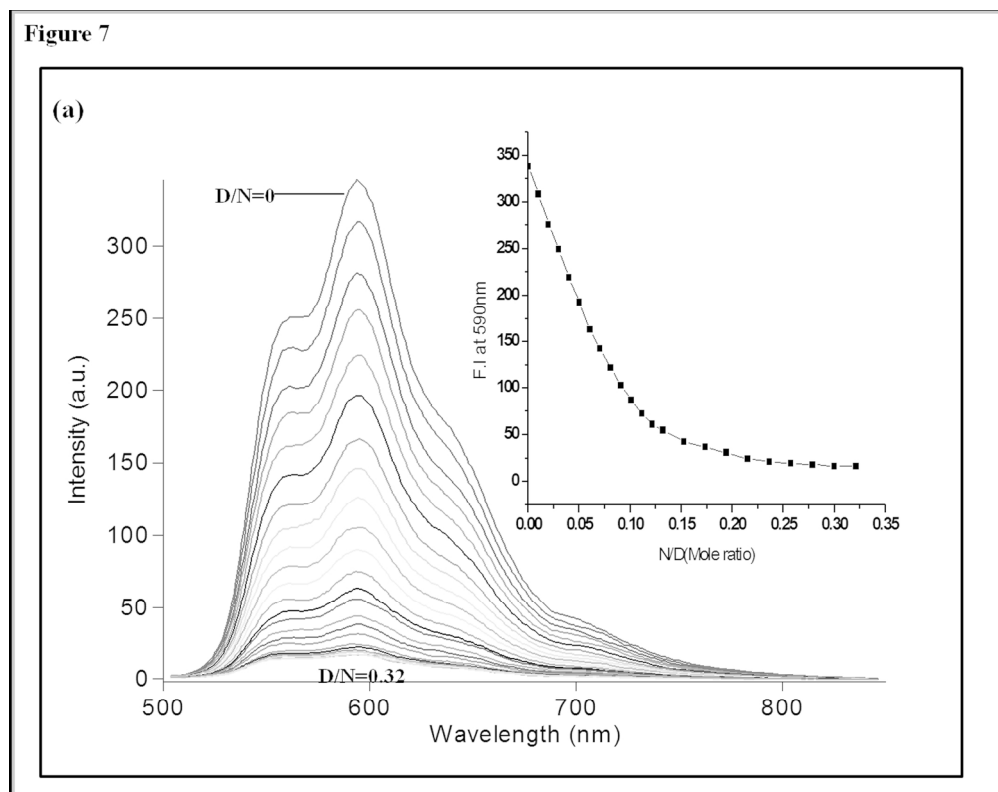
Figure 7: Spectrofluorometric titrations (a) (λexc, 480 nm) of adriamycin (10 μM) and (b) (λexc, 380 nm) actinomycoin(10 μM) with increasing concentration of 25R*R●Y triplex at N/D mole ratios ranging from 0.0 to 0.32 and 0.0 to 0.67 respectively. (inset) Changes in fluorescence intensity of adriamycin at 590 and actinomycin at 480nm as a function of N/D.
181x142mm (300 x 300 DPI)
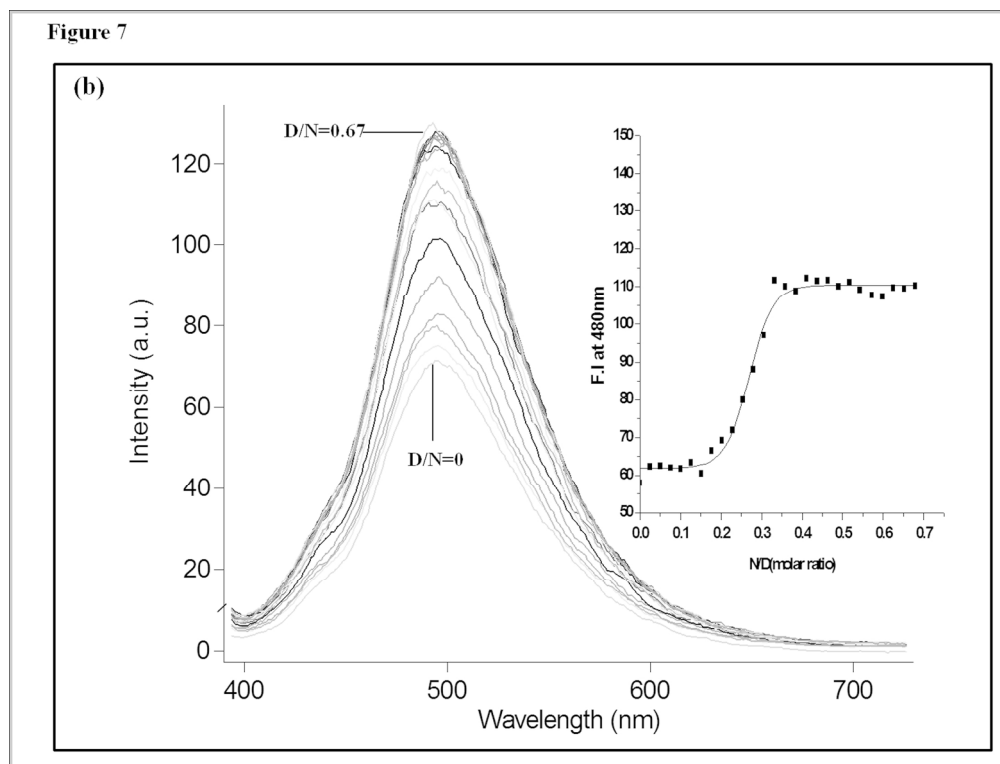
Figure 7

Figure 7: Spectrofluorometric titrations (a) (λexc, 480 nm) of adriamycin (10 µM) and (b) (λexc, 380 nm) actinomycoin(10 µM) with increasing concentration of 25R*R•Y triplex at N/D mole ratios ranging from 0.0 to 0.32 and 0.0 to 0.67 respectively. (inset) Changes in fluorescence intensity of adriamycin at 590 and actinomycin at 480nm as a function of N/D.
187x142mm (300 x 300 DPI)
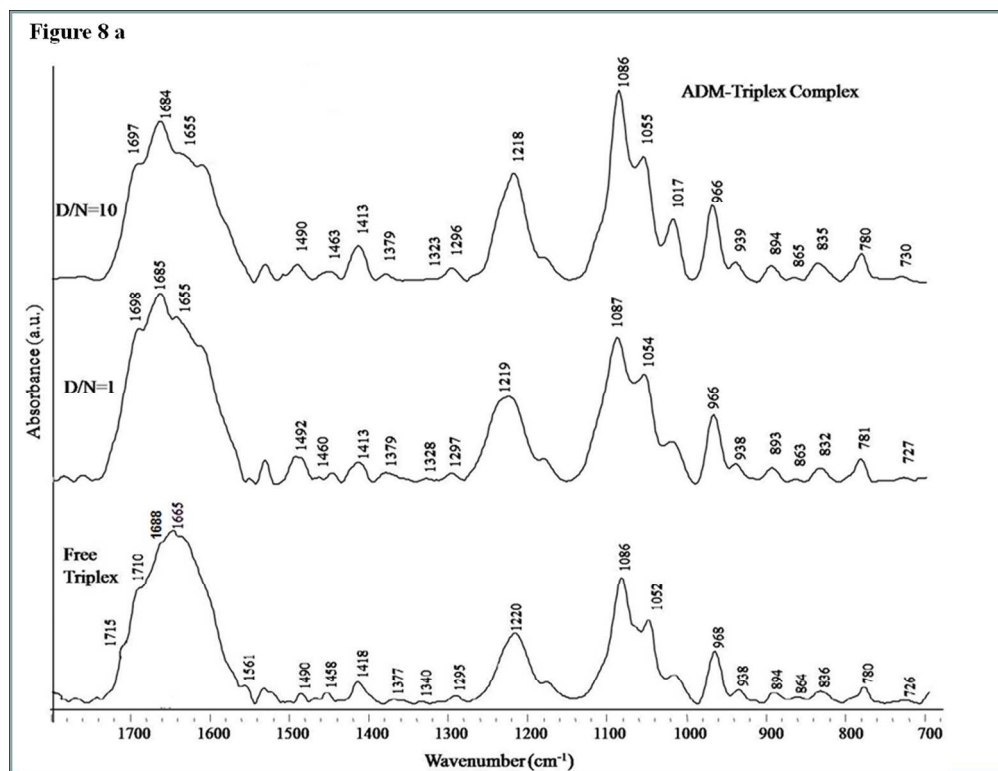
Figure 8: (a) FTIR spectra of 25R*R•Y solution and its complex with ADM solution at D/N=1 and 10
in 10mM Na-cacodylate buffer containing 120mM NaCl and 10 mM MgCl$_2$ at pH 7.0 in the region of 1800
to 700 cm^{-1}.(b) The FTIR difference spectra of triplex- ADM [(25R*R•Y solution + ADM solution) – 25R*R•Y
solution] at D/N=1 and 10.
191x146mm (300 x 300 DPI)
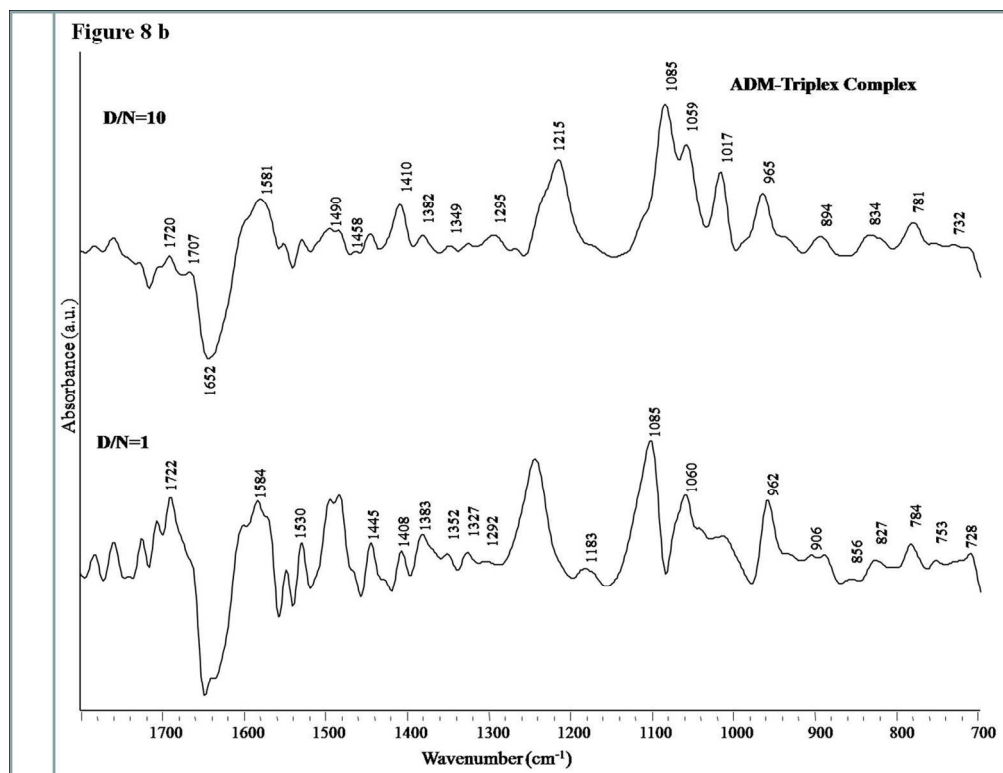
Figure 8: (a) FTIR spectra of 25R*R•Y solution and its complex with ADM solution at D/N=1 and 10 in 10mM Na-cacodylate buffer containing 120mM NaCl and 10 mM $MgCl_2$ at pH 7.0 in the region of 1800 to 700 cm^{-1}.(b) The FTIR difference spectra of triplex- ADM [(25R*R•Y solution + ADM solution) − 25R*R•Y solution] at D/N=1 and 10.
189x145mm (300 x 300 DPI)
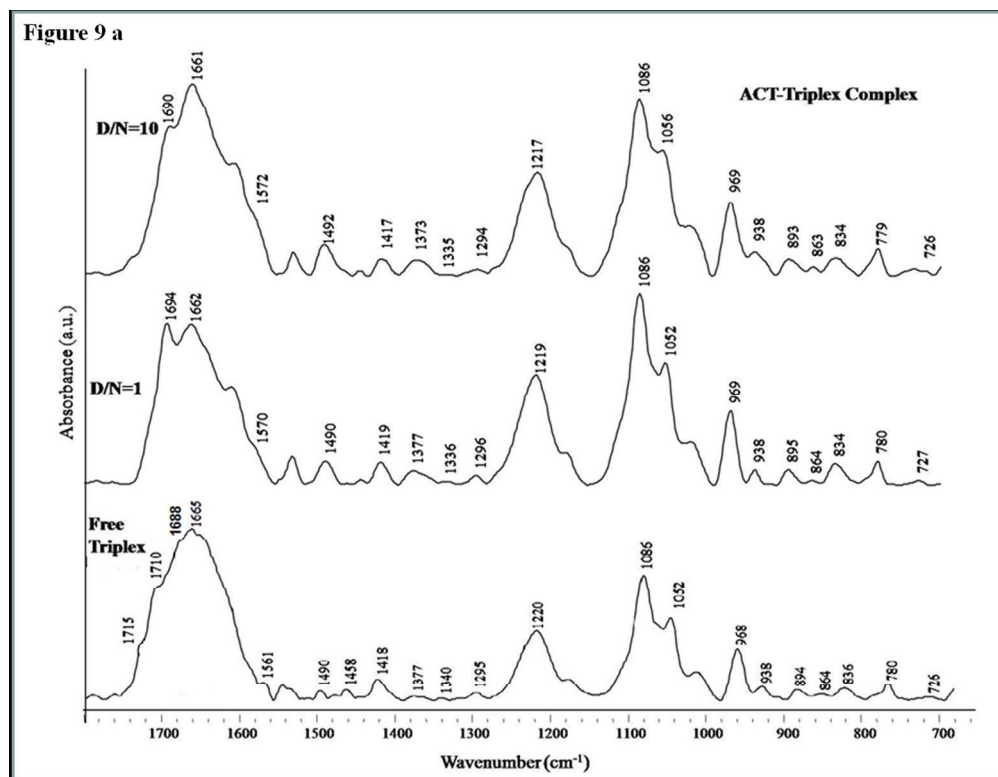
Figure 9: (a) FTIR spectra of 25R*R•Y solution and its complex with ACT solution at D/N=1 and 10 in 10 mM Na-cacodylate buffer containing 120mM NaCl and 10 mM MgCl$_2$ at pH 7.0 in the region of 1800 to 700 cm^{-1}.(b) The FTIR difference spectra of triplex- ACT [(25R*R•Y solution + ACT solution) − 25R*R•Y solution] at D/N=1 and 10.
185x142mm (300 x 300 DPI)
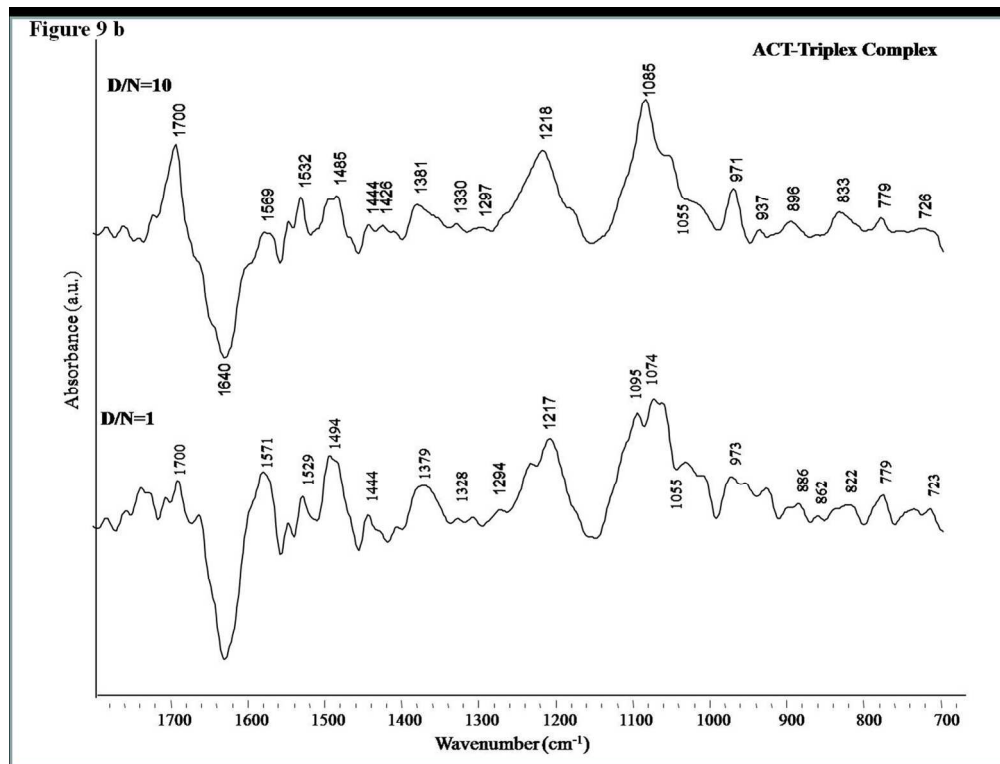
Figure 9: (a) FTIR spectra of 25R*R•Y solution and its complex with ACT solution at D/N=1 and 10 in 10mM Na-cacodylate buffer containing 120mM NaCl and 10 mM $MgCl_2$ at pH 7.0 in the region of 1800 to 700 cm^{-1}.(b) The FTIR difference spectra of triplex- ACT [(25R*R•Y solution + ACT solution) − 25R*R•Y solution] at D/N=1 and 10.
193x147mm (300 x 300 DPI)
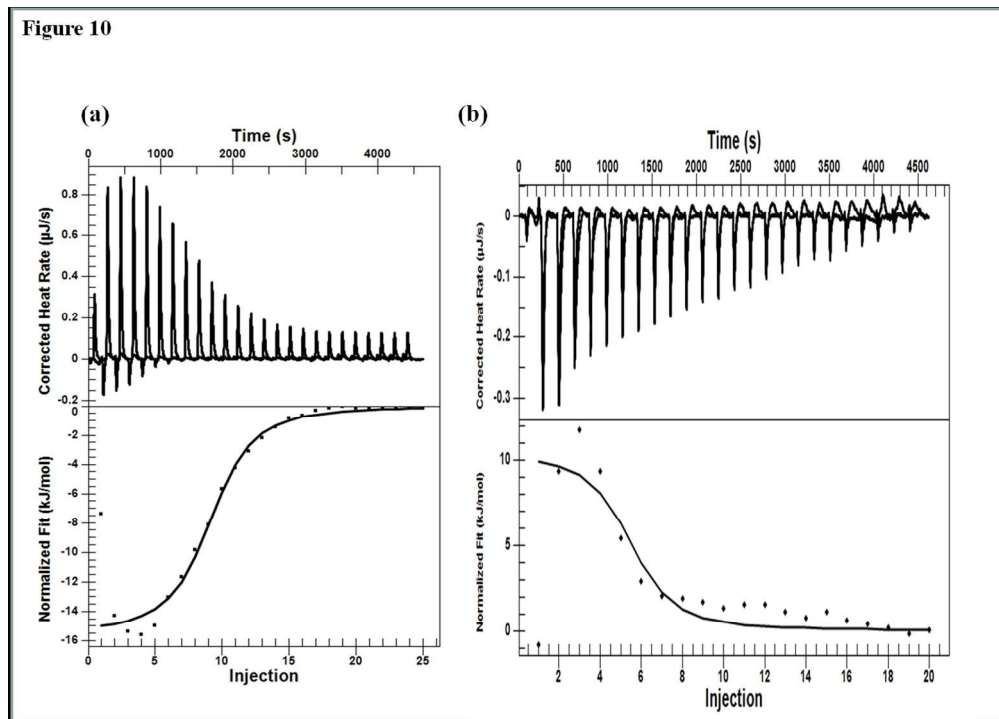
Figure 10: Representative ITC profile for 5µM 25R*R•Y interaction with (a) (600µM) ADM and (b) (450µM)ACT solution in 10mM Na-cacodylate buffer containing 120mM NaCl and 10 mM MgCl$_2$ at pH 7.0 at 25ºC. The small spikes in the ITC profile (upper panel) represents heat of dilution correctioned by injecting the ligands into 25R*R•Y triplex -free buffer under identical experimental conditions and was subtracted from corresponding heat of the ligand–triplex complexation.
183x131mm (300 x 300 DPI)

Table 1: Binding parameters of ADM and ACT complexation with 25RYduplex, 25R*R●Y
 triplex interaction using UV-VIS spectrophotometer in 10mM Na-cacodylate buffer
containing 120mM NaCl and 10 mM $MgCl_2$ at pH 7.0 at 25ºC.

Parameters	25RY duplex-ADM	25R*R●Y triplex -ADM	25RY duplex-ACT	25R*R●Y triplex -ACT
$Ka(M^{-1})x10^5$	2.0	18	4.2	52
Hypochromicity (%)	40	64	25	55

Table 2: Thermodynamic parameters of ADM and ACT complexation with 25RY duplex and 25R*R●Y triplex along with TFO – duplex interaction in 10mM Na-Cacodylate buffer containing 120mM NaCl and 10 mM $MgCl_2$ at pH 7.0 at 25°C.

Complex	n (Stoichiometry)	Binding affinity $Ka(/M) \times 10^5$	Enthalpy change $\Delta H(kJ/mol)$	Entropy change $\Delta S(J/mol\ k)$	Free energy change $\Delta G\ (kcal/mol)$
25RY duplex + 19 RTFO	1±0.1	750 ±300	-57±3.3	-40	-10
25RY duplex+ ADM	n1 =10.0 ± 2 n2 = 7 ± 2	Ka_1 = 1.3 ± 1 Ka_2 = 5.2 ± 1.4	dH1= −172. 5 ± 40 dH2= −137 ± 36	dS1 = − 480 dS2 = − 352	ΔG1=-6.94 ΔG2= -7.7
25RY duplex + Act-D	4± 1	0.6±0.3	17. 3±2.3	149.6	-5.13
25R*R●Y triplex +ADM	n1 =8.0 ± 1 n2 = 4.9 ± 2	Ka_1 = 8500± 300 Ka_2 = 720 ± 500	dH1= −159. 5 ± 30 dH2= −5 ± 29	dS1 = − 365 dS2 = 131	ΔG1=-12.1 ΔG2= -10.6
25R*R●Y triplex +Act-D	N=5±0.5	6.9±0.7	10.5±2	147	-7.3